ADVANCED MATERIALS
www.advmat.de

Molecular Engineering of 2D Nanomaterial Field-Effect Transistor Sensors: Fundamentals and Translation across the Innovation Spectrum

Junhong Chen, Haihui Pu, Mark C. Hersam, and Paul Westerhoff*

Over the last decade, 2D layered nanomaterials have attracted significant attention across the scientific community due to their rich and exotic properties. Various nanoelectronic devices based on these 2D nanomaterials have been explored and demonstrated, including those for environmental applications. Here, the fundamental attributes of 2D layered nanomaterials for field-effect transistor (FET) sensors and tunneling FET (TFET) sensors, which provide versatile detection of water contaminants such as heavy-metal ions, bacteria, nutrients, and organic pollutants, are discussed. The major challenges and opportunities are also outlined for designing and fabricating 2D nanomaterial FET/TFET sensors with superior performance. Translation of these FET/TFET sensors from fundamental research to applied technology is illustrated through a case study on graphene-based real-time FET water sensors. A second case study centers on large-scale sensor networks for water-quality monitoring to enable intelligent drinking water and river-water systems. Overall, 2D nanomaterial FET sensors have significant potential for enabling a human-centered intelligent water system that can likely be applied to other precarious water supplies around the globe.

1. Introduction

The current unmet need for low-cost, real-time, sensitive, and selective detection of a wide range of analytes presents a key opportunity for innovation at the nexus of food-energy-water systems (INFEWS) through the use of sensor networks[1] and distributed information processing for next-generation smart and resilient infrastructure.[2] When they are economical and accurate, distributed sensor networks generate massive amounts of data at high spatio-temporal resolutions, which provide system feedback and predictive capabilities through the use of artificial intelligence (AI) and science-driven models.

A poignant example of this opportunity is the global need for sustainably clean and safe water supplies. Current water-quality monitoring for public water supply systems is frequently applied at the water-supply intake and the water treatment plant. It is much less frequently applied along the water distribution lines and at the point of use, which creates vulnerabilities if the water quality changes within a water distribution system. For example, a large portion of water pipes in the United States (US) public water systems are near the end of their useful life and are in unsatisfactory conditions.[3] In Flint, Michigan, corroded lead-based water pipes led to a public health crisis,[4] in which many residents had elevated blood lead levels from drinking tap water contaminated with lead that had leached from the corroded pipes.[5] Furthermore, it is estimated that more than 18 million people in US are served by 5363 community water systems that violated the Safe Drinking Water Act Lead and Copper Rule.[6] Since a diverse range of related water-supply issues are present throughout the industrialized and developing world, high-performance sensors and sensor networks have the potential for global impact on human health.

Conventional laboratory methods based on spectroscopy and chromatography can specifically and accurately determine contaminants in water, but they require expensive and sophisticated laboratory instrumentation, complicated sample preparation, and trained operators, making them unsuitable for large-scale and in situ monitoring and detection.[7] For example, inductively coupled plasma–mass spectrometry (ICP-MS) is presently the gold standard for measuring heavy metals in water (e.g., lead and mercury). Typical measurements involve water-sample collection following specific instructions and subsequent laboratory analysis, which costs tens of dollars per sample and takes hours or days from sample to data.[8] On the other hand,

J. H. Chen, H. H. Pu
Pritzker School of Molecular Engineering
University of Chicago
Chicago, IL 60637, USA
E-mail: junhongchen@uchicago.edu
J. H. Chen, H. H. Pu
Chemical Sciences and Engineering Division
Physical Sciences and Engineering Directorate
Argonne National Laboratory
Lemont, IL 60439, USA
M. C. Hersam
Department of Materials Science and Engineering and Department of Chemistry
Northwestern University
Evanston, IL 60208, USA
P. Westerhoff
School of Sustainable Engineering and The Built Environment
Arizona State University
Tempe, AZ 85287, USA
The ORCID identification number(s) for the author(s) of this article can be found under https://doi.org/10.1002/adma.202106975.

DOI: 10.1002/adma.202106975

in recent years, significant progress has been made toward the in situ detection of water contaminants using optical, electrochemical, and electronic sensors.[1,7] These advances suggest that in situ detection could be viable, but a trade-off often exists between performance and price. For instance, voltammetry[9] and fluorescence[10] are capable of quantitatively detecting lead in water down to the μg L^{-1} (ppb) level but with a hefty price ranging from hundreds to thousands of dollars. As a result, a massive unmet need remains for accurate and accessible detection technologies that enable real-time, onsite water-quality monitoring at the point of use or within a water distribution system for early warning of water contamination.

The field-effect transistor (FET)-based sensing platform has attracted growing attention in the last decade due to its advantages of high sensitivity, rapid response, low cost, and well-defined signal transduction, thus holding promise for large-scale and in situ detection. FET sensors can detect a wide range of analytes, including toxic gases, water contaminants, and biological species, with exceptionally high sensitivity, selectivity, and response time.[7] An FET sensor typically consists of a semiconductor channel, source and drain electrodes, top/bottom gate oxide/electrodes, and analyte-specific detection probes attached to the gate oxide or semiconductor channel. The external perturbation introduced by target analyte binding with detection probes modulates the semiconductor channel current, which is further transduced into a sensor signal by measuring the change in the FET electrical characteristics (e.g., conductance or resistance). In contrast to the FET architecture in which charge carriers move from the source to the drain electrode through a single channel material, the tunneling FET (TFET) structure relies on charge carriers tunneling through a heterojunction formed by two different channel materials. For both FETs and TEFT sensors, reduced thickness in the channel material generally improves the sensor response due to the higher electronic sensitivity to external perturbations caused by adsorbed analytes. Moreover, a decrease in the dimensionality of the semiconductor channel also changes the underlying material physics, which can introduce additional opportunities for optimizing sensing performance. Specifically, 2D nanomaterials are leading candidates for FET/TFET sensors due to their tunable properties, structural diversity, ease of integration due to intrinsic van der Waals bonding, and high surface-to-volume ratios. The family of 2D semiconductors provides diverse options ranging from zero-bandgap graphene[11] to finite-bandgap transition metal dichalcogenides (TMDs)[12] and phosphorene/black phosphorus (BP).[13] The properties of 2D nanomaterials can be exquisitely tuned by controlling thickness,[12a,13a] forming heterostructures,[14] or surface modification.[15] Recent studies have demonstrated that correlated electron phenomena can also be obtained by twisting the stacking angle of bilayer graphene, providing another opportunity for tuning the properties of the 2D-nanomaterial channel.[16]

Herein, we first discuss the physics of 2D layered nanomaterials for both FET and TFET sensors. In contrast to conventional FETs based on bulk covalently bonded semiconductors, the strong in-plane bonding and weak interlayer interactions endow 2D layered nanomaterials with high surface quality after exfoliation, leading to higher carrier mobility in the ultrathin limit.[17] The confinement of carriers within atomically thin layers also gives rise to more efficient gate electrostatic control.[18] In addition, 2D TFETs exhibit an exceptionally abrupt subthreshold swing (SS) due to sharp band edges and quantum confinement effects.[19] The wide range of bandgaps and band splitting in 2D semiconductors also enables high drive currents.[20] These diverse attributes contribute to the high sensitivity, fast response, and low energy cost of FET/TFET sensors. Beyond fundamental science, herein, we further consider the potential challenges for translating 2D-nanomaterial sensors from the research laboratory to widely deployed practical settings. Water-quality monitoring is used as a representative application through two case studies: one on the commercial translation of a graphene-based FET sensor and the other on testbeds for large-scale water-quality sensor networks.

2. Physical Attributes of 2D Nanomaterials for FET and TFET Sensors

FETs use a gate potential to electrostatically control charge carrier transport in a semiconductor channel. By solving the Poisson equation, the natural scaling length of the channel is given by $\lambda = \sqrt{t_{ch} t_{ox} \varepsilon_{ch} / \varepsilon_{ox}}$, where t_{ch} is the thickness of the semiconductor channel, t_{ox} is the thickness of the gate oxide, and ε_{ch} and ε_{ox} are the dielectric constants of the semiconductor channel and gate oxide, respectively.[21] The channel length can be shortened by either decreasing the thickness of channel or using a high-k (dielectric constant) gate oxide. For efficient electrostatic control of the carriers, the channel should be several times longer than the scaling length, otherwise hot carriers can migrate over the potential barrier and lead to leakage currents (**Figure 1**a), resulting in high static power and associated heat dissipation.

Traditional bulk semiconductors have 3D covalent bonding. Consequently, ultrathin bulk semiconductors possess surface dangling bonds and traps at the interface between the channel and gate dielectrics. These dangling bonds result in carrier scattering that increases power consumption and reduces response time. As the channel gets thinner, the carrier mobility μ typically decreases as the sixth power of the channel thickness ($\mu \propto t_{ch}^{6}$), whereas the bandgap increases quadratically ($\Delta E_g \propto t_{ch}^{-2}$).[22] In addition, trapped interface states form charge centroids with nanometer-scale dimensions,[23] which screen applied fields and degrade electrostatic gating. In contrast, 2D nanomaterials are promising for short-channel FETs due to their weak van der Waals interlayer interactions and passivated surfaces. After exfoliation, few to no dangling bonds are present, resulting in reduced carrier scattering compared to ultrathin bulk semiconductors. Moreover, trapped impurity charges can be minimized when 2D semiconductors are interfaced with 2D layered dielectrics, providing further carrier mobility enhancement, as evidenced by the improved mobility in MoS_2 by more than one order of magnitude after being passivated by 2D hexagonal boron nitride (h-BN).[24] The well-defined and uniform 2D semiconductor channel is efficiently modulated by the gate potential, with an electrostatic efficiency approaching ≈80% for MoS_2[25] compared with ≈40–50% for 3D bulk semiconductors.[26]

The advantages of 2D nanomaterials extend to the subthreshold regime of TFETs.[19] For a conventional FET,

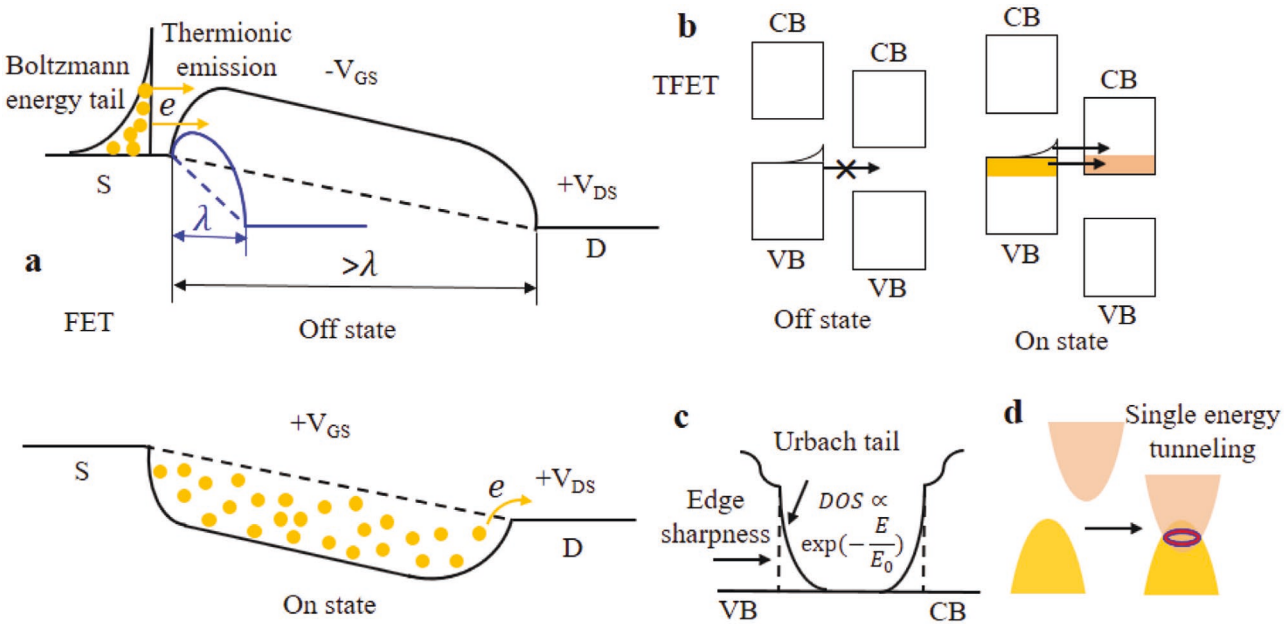

Figure 1. a) Schematic of operation in the on and off states for a conventional FET with an n-type semiconducting channel. The electrons move from the source to drain via thermionic emission, while the barrier height is controlled by the gate–source voltage (V_{GS}) (e.g., increased height by the negative voltage). Only when the channel length is much longer (typically >10λ) than the natural scaling length λ can the transistor be effectively turned off. Otherwise, the gate loses control over the barrier and the high-energy tail causes electrons to migrate over the lowered barrier, leading to leakage current. b) Illustrations of the on and off states in a TFET. Electrons from the valance band (VB) in the source tunnel into the conduction band (CB) in the drain when they overlap with each other. Without band overlap, the high-energy electrons are filtered by the bandgap above the VB maximum. c) Schematic of the Urbach energy tail along the band edges. Ideally, the band edges are sharp, as illustrated by the dashed lines. However, in real materials, the band edges are smeared by structural disorder, electron-phonon interactions, and imperfections in stoichiometry. The density of states (DOS) of the Urbach tail varies exponentially with the Urbach energy E_0. d) Diagram of electron tunneling for a 2D lateral TFET. Due to the quantum confinement of electrons along the tunneling direction, the electron energy is quantized in the quantum well with a limited number of energy states for atomically thin 2D nanomaterials. Single-energy tunneling occurs with conservation of both energy and momentum, as shown by the red circle in the overlapped bands, while the energy and momentum conservation restrictions can be lifted to some extent with the aid of phonons and defect states.

the carrier transport is dictated by thermionic emission over the gate-controlled barrier (Figure 1a). The drain current in a single-gate configuration thus changes exponentially with voltage ($I \propto \exp(eV/k_BT)$), thereby fundamentally limiting the SS to ≈60 mV per dec ($SS \propto k_BT/(e\ln 10)$) at room temperature. In contrast, for a TFET, carrier transport occurs through the barrier via interband tunneling from the valence band to the conduction band[27] across a heterojunction, which implies that the high-energy carriers are filtered by the bandgap above the valence band edge (Figure 1b). As a result, the SS in TFETs is governed by the band edge sharpness in the heterojunctions. Physically, the band edge in a semiconductor is not sharp due to an Urbach band tail inside the gap.[28] The density of states (DOS) in the band tail is inversely related to the Urbach tail energy (E_0) with an exponential form DOS ∝ $\exp(-E/E_0)$, such that smaller Urbach tail energies lead to sharper band edges (Figure 1c). Structurally speaking, the band tails in 3D heterojunctions can have a wide distribution (i.e., larger E_0) due to trapped states, lattice mismatch imperfections, spatial inhomogeneity in thickness, and random doping distribution in the lattice.[29] On the other hand, for 2D heterojunctions, the van der Waals interaction eliminates lattice-matching issues, and the atomically flat interface suppresses band edge roughness.[30] Regarding thermal disorder, 2D heterojunctions experience less band-edge smearing than 3D bulk heterojunctions due to weak electron–phonon interactions and low deformational potentials.

For TFETs, SS is proportional to the Urbach energy ($SS = 2.3E_0/e\eta$, where η is the gate coupling efficiency[26,31]). The calculated E_0 at a high current density (or large tunneling probability)[32] for bulk semiconductors is 22 meV for Si and 15 meV for Ge, whereas those of single-layer 2D semiconductors are considerably lower: 4 meV for MoS_2, 2 meV for $MoSe_2$, and 2 meV for BP. Therefore, the SS in heterojunction TFETs is predicted to follow the trend of 3D–3D > 3D–2D > 2D–2D.[32] These expectations from theory generally agree well with experiments as illustrated by the case of Ge–MoS_2 (bilayer), where the predicted SS of 3.2 mV per dec is close to the experimental value (3.9 mV per dec).[33] From a quantum mechanical perspective, confinement in a quantum well along the tunneling direction suggests a preferred step response function of conductance in 2D–2D vertical heterojunctions due to the simultaneous conservation of energy and momentum for a single tunneling energy (Figure 1d),[34] whereas the energy is broadened in higher dimensional heterojunctions (e.g., 3D–3D) where a quadratic relationship between current and voltage is predicted.[35] For 1D–1D heterojunctions with a point contact, the carrier transport along nanowires exhibits a linear response[35] in a manner where the nanowire radius has to be much smaller (≈nm) to achieve the same response as the 2D–2D counterpart.[33] This requirement poses challenges in the device fabrication for 1D nanomaterials, and thus 2D nanomaterials are the preferred option for TFETs.

Transistors based on 2D nanomaterials can also provide advantageous switching speed compared to 3D bulk materials with the same energy bandgap and/or carrier concentration. The delay τ in a transistor is characterized as $\tau = CV/I$, where C is the gate capacitance, V is the supply voltage, and I is the drive current. Faster switching speeds (i.e., smaller τ) require a larger drive current (assuming the same C and V), which depends on the intrinsic transport properties of the channel (e.g., carrier mobility and concentration). The larger carrier mobility in 2D layered nanomaterials is beneficial for higher drive currents. In addition, the splitting of valence subbands by up to hundreds of meV due to broken crystal symmetry in the out-of-plane direction and strong spin–orbit coupling exists in some 2D TMD semiconductors[20] in contrast to their bulk 3D counterparts. The effective mass in these valleys influences the ballistic transport in FETs. Particularly for smaller effective masses ($<0.2m_0$, where m_0 is the free electron mass), a larger number of valleys leads to a proportionately higher drive current.[36] For TFETs, the drive current depends more significantly on the carrier concentration, assuming the same tunneling probability and contact area. Therefore, a smaller bandgap in the channel is preferred without degrading the transfer characteristics since the off-state is obtained through forbidden band tunneling. In practice, this large drive current is more prominent than the switching speed when evaluating the performance of 2D-nanomaterial-based FET/TFET sensors. Fast-switching 2D-nanomaterial-based sensors operate with lower energy consumption since a smaller drain voltage is needed to achieve the same drive current, while the ultimate sensor response time is limited by the slower diffusion/transport of analytes onto the sensor surface to reach an equilibrium state, whose characteristic time is typically on the order of seconds in contrast to the intrinsic transistor switching time on the order of nanoseconds.

2D nanomaterials offer many bandgap choices ranging from semimetals to insulators, and thus a suitable bandgap can be achieved by selecting materials with proper band engineering based on thickness control. In contrast, reduced thickness in 3D bulk semiconductors can lead to both severe mobility degradation and bandgap increases, and thus the drive current will be compromised. To mitigate such effects, 3D bulk semiconductors in the source region of a TFET are usually heavily doped to enhance both the carrier concentration and electric field across the interface for carrier injection. However, this approach sacrifices SS due to doping-induced band-edge smearing.[37] For 1D nanomaterials derived from 2D nanomaterials by cutting or rolling, the reduced dimensionality limits the contact area with the electrode in a TFET, thus compromising the magnitude of the tunneling current and switching speed.

3. Sensor Design and Fabrication Based on 2D FETs/TFETs

FET/TFET sensors are based on monitoring the electrical resistance or conductance change induced by target adsorbates such as gases, ions, and biomolecules. The sensitivity can be derived from the transfer characteristics with the sensor operation mode lying either in the linear response or subthreshold region, where the carrier mobility and SS dominate the sensing mechanism, respectively (**Figure 2**a). The advantages of 2D nanomaterials over 3D bulk materials in terms of carrier mobility, SS, and switching speed translate into high sensitivity and fast responses for 2D FET/TFET sensors. For the same gate voltage change and on–off current ratio, the sensitivity can be enhanced with a larger carrier mobility and a smaller SS. In particular, the sensitivity depends linearly on carrier mobility and as the tenth power of SS, suggesting that TFETs are ideal for ultrasensitive detection. For example, a TFET biosensor has been demonstrated to show a higher sensitivity by more than four orders of magnitude and a shorter response time by one order of magnitude compared with a conventional FET sensor.[38]

To further employ the effect of carrier mobility, sensors can be designed by vertically stacking 2D nanomaterials,[14] separated by a small-bandgap 2D semiconductor (Figure 2b). The 2D separator acts as a barrier and can be tuned by the external top gate to control carrier transport. Practically, BN layers are used to screen the carrier-scattering charge impurities in the substrate and gate oxide. For TFET sensing, the tunneling current can be tuned by adjusting either the carrier overlap concentration with constant tunneling probability in the vertical architecture (Figure 2c) or the tunneling width with fixed carrier overlap concentration in the lateral architecture (Figure 2d). For both FET and TFET sensing, the external top gate can be realized by the adsorption of charged species to specific probes anchored to the gate oxide.

FET sensors also exhibit responses through direct contact between the adsorbates and 2D sensor materials. For example, both theory and experiments show that sensor performance for nitrogen dioxide is optimized at a thickness of a few nanometers for phosphorus nanosheets (PNS).[39] The dependence of the sensitivity on thickness can be categorized into two regimes. For thinner PNS with a thickness-dependent bandgap, the sensitivities are dictated by the bandgap. However, for thicker PNS, despite the invariant bandgap, its conductivity is governed by an effective thickness region after gas adsorption in the framework of a resistance network model, which increases gradually and finally saturates as the actual PNS thickness increases (**Figure 3**a).

Upon physical adsorption, charge transfer typically occurs for neutral gas molecules, whereas both charge transfer and electrostatic gating modulation occur for charged adsorbates such as metal ions in aqueous environments. These two regimes (i.e., charge transfer versus electrostatic gating in Figure 3b) are predicted and observed in PNS sensors, depending on the Debye screening length and the distance between adsorbed mercury ions.[40] At a lower adsorption density, the charge transfer effect is dominant, whereas the evolution from charge transfer to the electrostatic gating effect occurs at a higher adsorption density as the distance between adsorbed ions approaches the PNS Debye length.[40] The correlations between the sensor performance and the PNS intrinsic properties suggest that the lower detection limit can be predicted with the knowledge of the electronic properties of the sensor materials and its interaction strength with adsorbates. In addition, the sensor response range can be expanded from an ultralow to an ultrahigh concentration of adsorbates in an array of sensors or sensor network with sensing materials in different thicknesses.

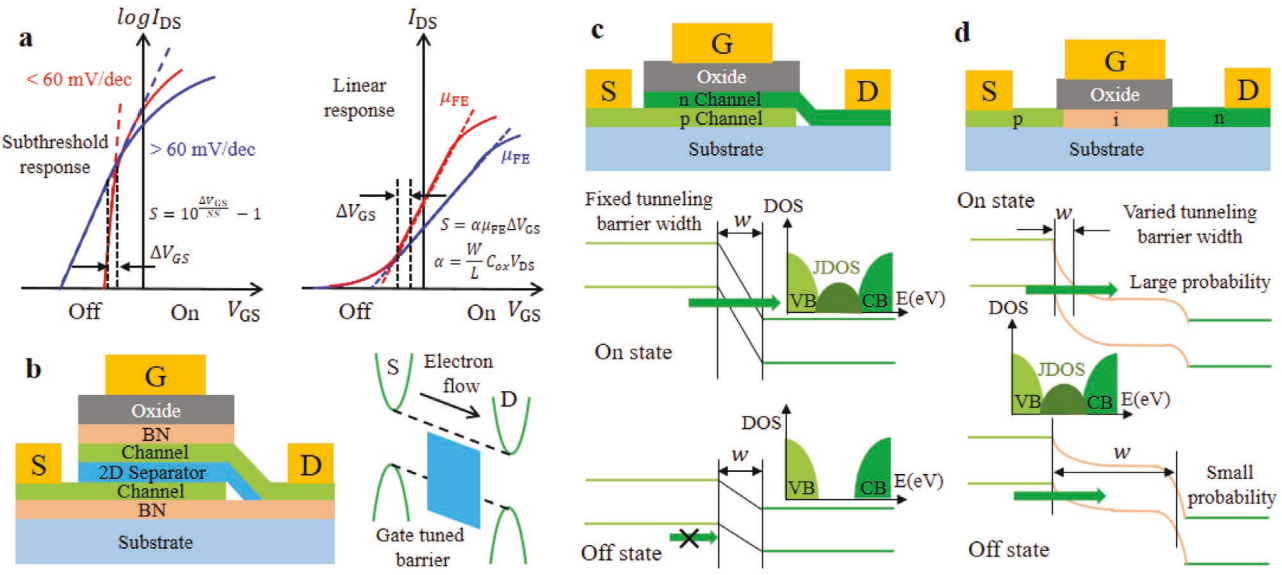

Figure 2. a) Schematic transfer characteristics of an FET and TFET for log and linear scales of drain–source current I_{DS} to visualize the subthreshold and linear responses, respectively. The SS is >60 mV per dec for FETs due to the thermionic emission of electrons, while it is <60 mV per dec for TFETs resulting from band-to-band tunneling. In the subthreshold regime, the sensitivity S varies as the tenth power, and thus will be much larger for smaller SS with the same change of gate voltage (ΔV_{GS}). In the linear regime, S is linearly proportional to the product of field-effect carrier mobility μ_{FE} and gate voltage change ΔV_{GS}. The coefficient α depends on the channel width (W), channel length (L), gate oxide capacitance (C_{ox}), and drain–source voltage (V_{DS}). b) Illustrations of a 2D FET in a vertical heterostructure and band diagrams for electron transport. In the heterostructure, the channel is separated by a 2D semiconductor with suitable bandgap and band alignment. Boron nitride (BN) layers are used to mitigate the carrier-scattering on the surface of the substrate/gate oxide and thus enhance the carrier mobility. The electron flow can be tuned by the gate-controlled barrier from the 2D separator. c,d) Schematic structures and band diagrams of vertical and lateral 2D TFETs, respectively. For the vertical 2D TFET, the electrons from the VB in the p-doped source tunnel into the CB in the n-doped drain with a fixed tunneling barrier width since the distance between the p and n channels after direct contact is constant and small. The tunneling probability is the same for the on and off states since the tunneling current depends only on the joint DOS (JDOS) resulting from band overlap. In contrast, the JDOS is the same for both the on and off states in a lateral 2D FET, while the tunneling barrier width is tuned by the gate. The shortened barrier width gives rise to a large tunneling probability, and the electrons in the p-doped source tunnel through the intrinsic channel into the n-doped drain. Similarly, the probability becomes extremely small when the barrier width is widened by the gate and band-to-band tunneling is prohibited.

Note that 2D nanomaterials as the sensor channel in the FET/TFET structure lead to high sensitivity rather than high selectivity. Although a 2D nanomaterial can be specific to certain types of analytes after direct contact (e.g., MoS_2 and BP can specifically detect mercury ions as a result of the larger electronegativity of mercury compared to other interfering ions,[40,41] while NO_2 as a strongly oxidizing gas can be specifically detected by MoS_2, BP, and graphene[39,42]), this selectivity cannot be generalized to other analytes. Instead, molecular engineering of probes for selective binding with target analytes is required to exploit and expand the functionalities of FET/TFET sensors for accurate detection of various analytes with superior sensitivity and selectivity. The selectivity of an FET sensor can be tuned by decorating analyte-specific probes on the surface of the gate oxide or semiconductor channel. For gases, the probes are usually metal or metal oxide nanoparticles,[43] which are judiciously designed to provide appropriate band alignment among the sensor material, nanoparticles, and gas molecules, as illustrated in Figure 3c. The charge transfer between the gases and probes affects both the carrier concentration and the depth of charge depletion/accumulation regions, which act as scattering centers for carrier transport. The sensor performance is optimized with respect to the probe density by balancing the carrier concentration and mobility changes.

For charged analytes, the probes are typically molecules with desired functional groups. The identification of effective molecular probes requires careful study of the characteristic interactions between functional groups in the probe and target analytes. For example, mercury and lead ions prefer binding with amine and phosphate groups, and thus DNAzyme and DNA can be used as probes for detecting mercury and lead ions, respectively.[44] The carboxylic group in the short carbon chain conjugated on gold nanoparticles via the thiol group, such as dithiothreitol[45] and reduced glutathione,[46] can also be used for detecting heavy-metal ions. Depending on the pH, the functional groups in the molecular probe can be either protonated or deprotonated and thus positively and negatively charged, respectively. Evidently, the negatively charged state is favored in order to attract positively charged metal ions. Further opportunities also exist in the design and synthesis of new probes through macromolecular engineering. The identified molecular probes can be anchored directly to the sensor surface or to metal nanoparticles.[47] In this case, the sensor operates via a gating effect due to the charged nature of adsorbates, where the Debye length (Figure 3d) in the electrolyte influences the sensor performance.[48] Probes with a short chain or ligands are especially preferred in aqueous environments typically with a short Debye screening length. A more challenging but exciting opportunity lies in the design of a

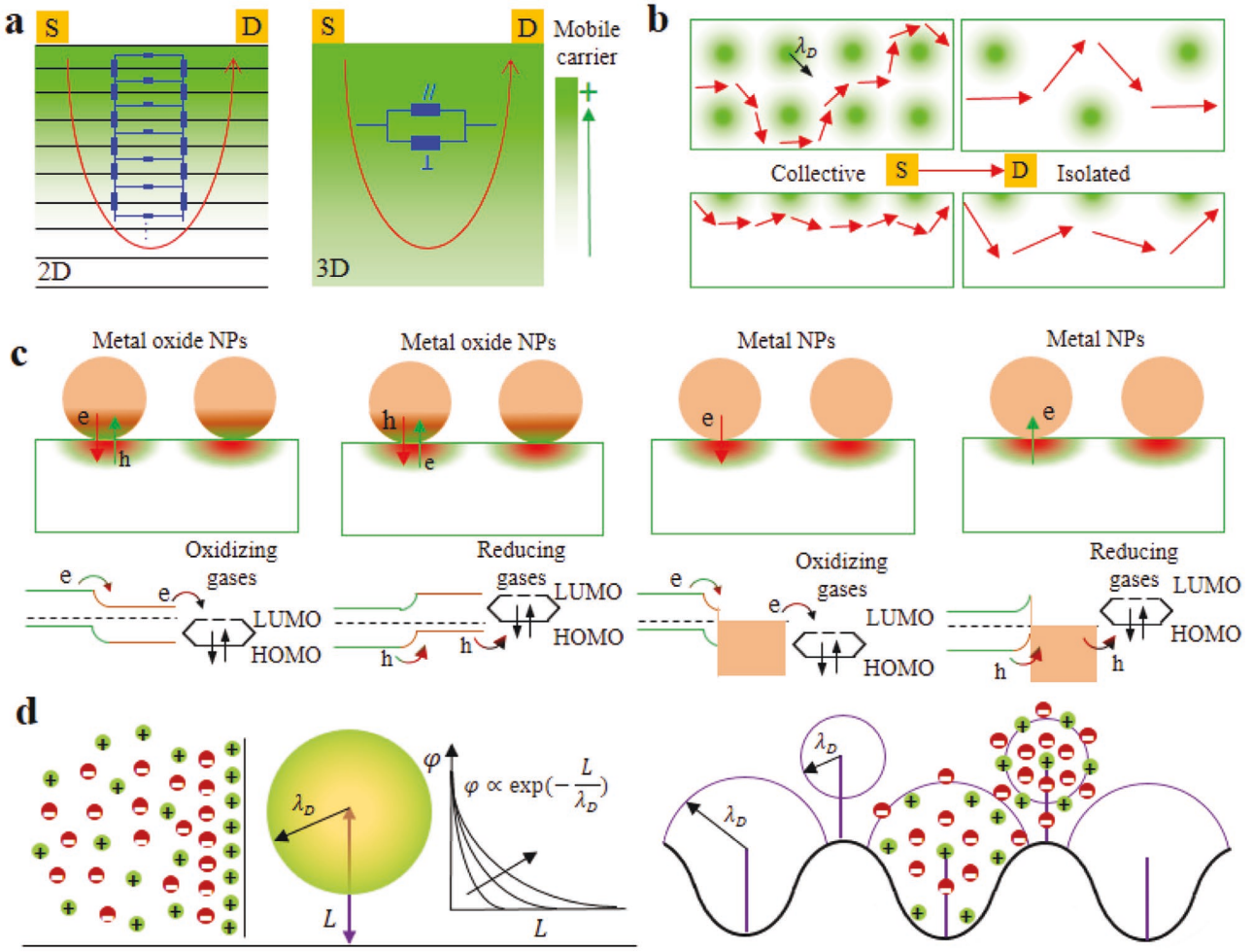

Figure 3. a) Schematic contour of mobile carrier concentration in 2D nanomaterial (solid black line indicates an individual layer) and 3D bulk semiconductors, assuming the same vertical thickness and bandgap. Modulation of the carrier concentration can result from either charge transfer or gating effects in a sensor. The red curved arrow indicates the direction of the electric field line along which carriers are transported. The inset shows the resistance network model with different electrical resistances along the plane (//) and out of plane (⊥) for 2D and the same for 3D. b) Top and side views of carrier transport due to the surface adsorbates at large (left) and small (right) densities in a 2D nanomaterial sensor. Within the Debye sphere with radius λ_D (green color), the carrier undergoes strong scattering and frequently changes its transport direction. c) Schematic interactions between metal oxide or metal NPs and 2D nanomaterials for gas sensing. The illustrated band diagrams present the path of charge transfer between the gas molecules (oxidizing vs reducing) and 2D nanomaterials via NPs. At the contact region, a p–n heterojunction forms between the p-type nanomaterial and n-type metal oxide NPs. For contact with the metal NPs, the junction is dominant in the semiconducting nanomaterial due to the large electron density in metal NPs. The carrier transport directions across the junction depend on the work function alignment. The lowest unoccupied molecular orbital (LUMO) accepts electrons for oxidizing gases, and the highest occupied molecular orbital (HOMO) donates electrons for reducing gases. d) Design principle for detecting charged species via the gating effect in a 2D FET or TFET sensor. For a 2D nanomaterial (left), the probe length L should be at least shorter than the Debye radius λ_D in the aqueous environment, otherwise, the carriers in the 2D nanomaterial cannot undergo a pronounced electric perturbation from the specific binding between the probe and charged adsorbates due to Debye screening. This screening effect can be mitigated in an exponential way with a larger Debye radius. For a crumpled 2D nanomaterial (right), the Debye radius is larger in the concave versus convex regions, which is promising for overcoming the Debye screening limit. The distribution of charged red and green balls depicts the electric double-layer formation.

moderate interaction strength between the molecular probe and the target analyte to achieve the reversible binding that is required for continuous or inline detection.

Historically, it has been assumed that high surface-to-volume ratios enhance the sensitivity of FET-based biosensors, which led to significant efforts to use nanowires for biosensing.[49] However, numerical simulations of nanowires on a substrate show that the enhanced sensitivity is due to reduced screening in concave corners, which implies that smaller diameter nanowires are less effective unless they are placed on an insulating substrate.[50] In the corners between the nanowire and the substrate, the electrolyte exhibits weaker Debye screening, leading to a larger charge sensitivity. Consequently, crumpled 2D nanomaterials[51] are effective for detecting charged analytes when using probes with long ligands that overcome the Debye length limit (Figure 3d). Compared with FETs, the lower SS in a TFET sensor results in a larger current change at the same target analyte adsorption density, which is

important in many cases where the surface potential modulation is only tens of mV.

Currently, most initial demonstrations in research laboratories fabricate sensors with single 2D nanomaterial flakes, which involves identifying the flake on the wafer followed by an aligned lithography step for electrode patterning. This laborious procedure is evidently too cumbersome and time-consuming for the commercialization of a sensor platform due to its low yield and a high cost. Solution-based exfoliation is promising for the large-scale production of few-layer 2D nanomaterials.[52] Following solution-based exfoliation, thin films can be achieved by spin coating or related liquid-phase deposition techniques, after which interdigitated electrodes can be patterned at any point on the substrate. Despite the scalability of this approach, the thickness and shape variations of 2D nanomaterials and their solution-deposited thin films[53] pose a significant challenge for the uniformity of electronic properties across the substrate surface, which compromises the homogeneity of the sensor array response. Therefore, improvements in the electronic uniformity and thin-film deposition of solution-processed 2D nanomaterials will expedite the commercialization of 2D-nanomaterial-based sensor technologies.[54] Another possibility is to accommodate device-to-device inhomogeneity by using calibration algorithms that take advantage of advanced data-mining techniques. For example, with the framework of state-of-the-art machine learning (ML), a feed forward neural network can learn and exploit the unique response of each sensor in the array by taking into account both the structural and electronic characteristics of the sensors.

The top-gate oxide of an FET/TFET is typically fabricated by atomic layer deposition.[55] For a given dielectric material, a thinner gate oxide implies a larger capacitance and thus is favored for enhanced sensor response, but it provides less protection as an encapsulation layer.[56] To mitigate the degradation of the sensor response and enhance its lifetime, a thicker oxide can be used. However, a tradeoff has to be made between the sensor stability and the sensitivity because a thicker oxide increases the stability of the device at the cost of a lowered sensitivity and elevated limit of detection. One way to optimize this tradeoff is to employ high-k dielectrics for the gate oxide[57] (e.g., Al_2O_3 or SiO_2 can be replaced with HfO_2). Another promising option is to use multilayers of different gate oxides (e.g., Al_2O_3/TiO_2), which increases both the lifetime[58] and dielectric constant.[59]

4. Case Studies for Water-Quality Monitoring

As discussed above, 2D layered nanomaterials offer exciting opportunities to engineer FET/TFET sensors because their unique features (e.g., rich bandgap options, high carrier mobility, large gate electrostatic efficiency, and low SS) can potentially lead to superior sensing performance (e.g., ultralow limit of detection, high sensitivity, fast response, and natural integration with control electronics). In addition, the miniaturized FET/TEFT sensor chip and conductance-based measurements require less complicated hardware and circuit design for convenient integration into the existing water equipment and network. Prior success in FETs for microelectronics applications further suggests a scalable pathway toward low-cost manufacturing of such devices. Consequently, FET/TFET sensors have immense potential in quantitative onsite detection and monitoring of water quality at a large scale with facile operation. While FET sensors have been demonstrated in the past decade for ultrasensitive, versatile detection of chemical and biological analytes,[7] TFET sensors are still in their infancy due to relatively more complicated architecture and fabrication requirements compared with FET sensors.

In this section, we present two case studies on exploring 2D nanomaterial FET/TFET as emerging water-quality sensing technologies. Case study I will discuss the general roadmap and illustrate critical steps with potential roadblocks in the commercialization trajectory of a graphene-based FET water sensor for detecting heavy-metal ions. The discussion will focus on how the Technology Readiness Level (TRL) can be elevated from the concept formulation to prototyping and product realization by leveraging various funding mechanisms at the US National Science Foundation (NSF) and partnerships with the water industry, offering insights into how one can effectively embark on such a journey to translate other 2D-nanomaterial-based FET and emerging TFET sensor technologies. Case study II then envisions intelligent water systems and how the real-time FET/TFET sensor technologies can be deployed and tested in large-scale sensor networks through two potential testbeds, one for drinking water-quality monitoring and the other for geospatial mapping of river-water quality. These real-world applications not only motivate the research and development of 2D nanomaterial FET/TFET sensors but also illustrate the desirable performance metrics for these sensors, such as simultaneous detection of multiple contaminants, real-time monitoring, and sensor stability against biofouling effects.

4.1. Case Study I: Translation of a Graphene-Based FET Heavy-Metal-Ion Sensor Technology

Taking an original scientific discovery from the laboratory to the marketplace for real-world application is a complex and phased process that requires not only research (e.g., exploratory and fundamental studies) but also business activities (e.g., customer discovery and market survey). During the translation of a technology, its progress is often assigned with different maturity levels. In the US, particularly for government-funded technologies, TRLs are commonly used to quantitatively estimate this maturity level. TRLs are numbered from 1 (i.e., basic principles observed and reported) to 9 (i.e., actual system proven through successful mission operations or commercialization).[60] The general roadmap for technology translation can simply follow the TRL spectrum from 1 to 9. The involved critical steps include the invention of new technology, customer discovery to understand market needs, proof-of-application research, prototyping through partnership with industry, and product development and manufacturing. A vibrant innovation ecosystem that facilitates strategic partnerships with industry is the key to accelerating this process. Here, we illustrate such a journey to translate a graphene-based FET sensing technology from the laboratory to the marketplace, i.e., effectively elevating the TRL value by leveraging various funding mechanisms offered by the US NSF[61] (**Figure 4**a).

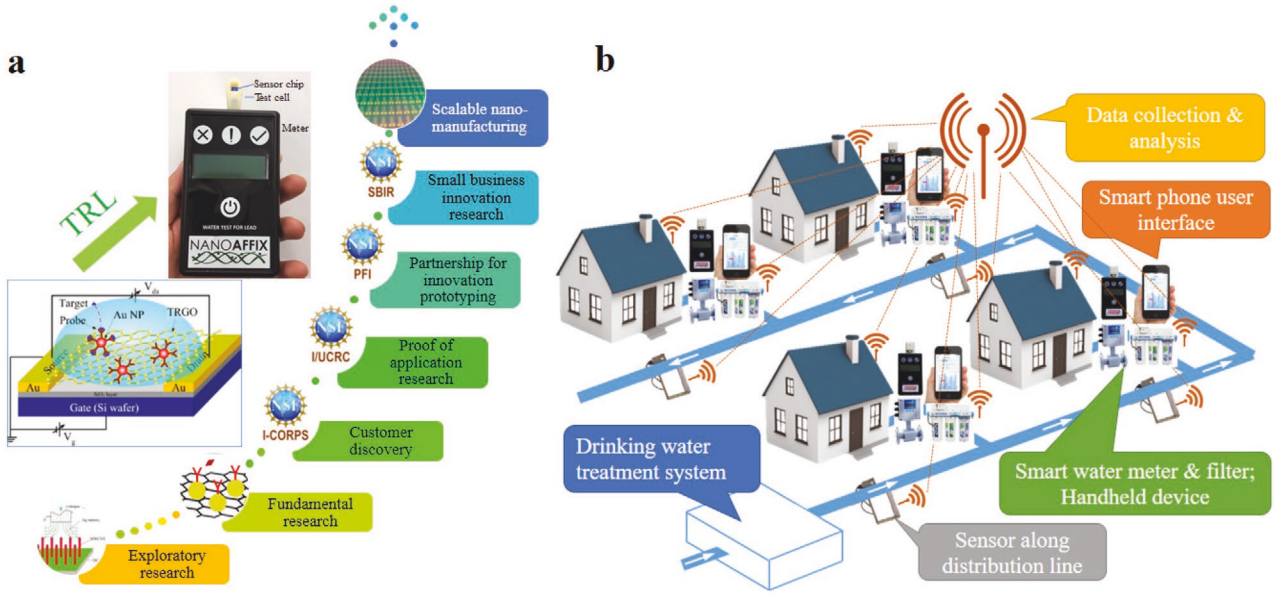

Figure 4. a) Illustration of the TRL evolution for a graphene-based FET sensor technology from exploratory research to scalable manufacturing. b) Schematic of an envisioned smart drinking-water system that integrates real-time sensing technologies throughout the system to continuously monitor water quality and quantity and to provide early-warning/alarm capabilities. In-line sensors are installed along water distribution lines and at households to enable the continuous monitoring of water quality and quantity. End-users are provided with handheld devices for regular water-quality testing at the point of use (POU). Sensing data/signals from both in-line sensors and handheld devices are collected, transmitted to a central control station (or cloud), and processed so that the entire water distribution system can be monitored and controlled remotely in real time by the water utility. Users can also access the information through smart phone apps and websites. If there is a warning triggered by elevated concentrations of certain contaminants, the system will automatically take measures to manage the situation and notify users who may be affected.

The invention of the FET sensing technology was made during a fundamental research project that discovered that the electrical characteristics of a graphene-based FET can be modified by electronic perturbations induced by binding events between analytes in the surrounding environment and the molecular probes functionalized on the FET device surface.[47b,62] The initial proof of concept for the FET sensing platform was demonstrated by the detection of proteins.[47b] The FET sensing technology soon attracted significant attention from the sensing and the nanomaterials communities, which motivated us to explore a critical pathway to bring the technology to the marketplace, particularly through industrial partnerships.

Initial conversations with water industry leaders suggested that the invented graphene-based FET sensing technology may be useful for detecting water contaminants such as heavy metals and bacteria. To identify the product-market fit and assess the potential for commercialization, a series of customer discovery interviews were conducted with potential customers of the technology in the water sector, which was sponsored by the NSF I-Corps program. More than 100 potential customers of the FET sensor technology were interviewed, which led to the conclusion that none of the existing sensing methods were desirable for water users and water service providers to perform low-cost, real-time, in situ detection of heavy metals in water. Therefore, an unmet need was identified for a fast, sensitive, selective, easy-to-use, and cost-effective method for detecting heavy metals. Graphene-based FET sensing technology could potentially meet this need and serve a sizable niche market.

Equipped with the customer discovery insights, the next critical step was to carry out the proof-of-application research. With support from the NSF Industry/University Cooperative Research Center (I/UCRC) program, the graphene-based FET sensor demonstrated promising features for in situ detection of heavy metals in water, such as rapid response (within seconds), high sensitivity and selectivity, ease of use, and low cost. Specifically, the graphene-based FET sensor was found to effectively detect heavy-metal ions in water (e.g., Pb^{2+} and Hg^{2+}) well below their action levels (e.g., 15 ppb for Pb^{2+}).[44a,46,47] While such a low limit of detection is encouraging, technical challenges needed to be resolved prior to real-world applications. For detecting water contaminants, more attention should be paid to mitigating interfering effects such as pH, hardness, disinfection byproducts, and particulates in various types of water. Heavy-metal ions in drinking water exist in the forms of free ions, complexed ions, and particulates, depending on the pH.[63] Therefore, pH dependence needs to be considered in optimizing the sensor response to accurately predict heavy metals in water. To detect all three forms of heavy metals, one potential solution is to establish the equilibrium model of the metal species and its dissolution kinetics with respect to pH,[64] and thus the total metal can be extrapolated from the dissolution curve against both time and pH.

The identified potential for commercialization and successful proof-of-application outcomes brought together several strategic water industry partners to prototype the technology with support from the NSF Partnerships for Innovation (PFI) program, which resulted in a functioning prototype handheld device for detecting heavy-metal ions in tap water. The prototype

handheld device is being commercialized by a start-up company through Small Business Innovation Research (SBIR) projects. In addition, scale-up manufacturing of the graphene-based FET sensor chip is being explored with support from the NSF Scalable Nanomanufacturing (SNM) program. In addition to the static detection by the developed handheld device for end-users, the water industry partners are also highly interested in integrating the developed sensor chips into the existing water infrastructure (e.g., water filters) with sufficient flexibility and adaptability for continuous monitoring of water quality. This goal brings about the issues of sensor stability and biofilm formation that will limit the lifetime of sensor and its function. It is also necessary to expand the detection spectrum of sensors to cover emerging water contaminants (e.g., pharmaceuticals, personal care products, endocrine-disrupting compounds, and microplastics).

4.2. Case Study II: Potential Water Sensor Testbeds for Intelligent Water Systems

Current methods for assessing the impact of pollution on water quality and its derivative impact on the environment and economy, as well as methods for quantifying issues of transparency, regulation, and measurement protocols, remain unsatisfactory due to a lack of adequate data. To address these problems, the availability of a wide variety of sensors offers the ability to develop effective cyberphysical sensor networks. In addition, it requires improvements in technologies related to the Internet of Things and network infrastructure. While drinking water can be contaminated by aging water pipes containing lead and copper, river waters worldwide are often polluted from industrial effluents, mine-tailings, municipal wastewater discharges, public recreation, and agricultural runoff. Significant examples of these pollutants include heavy metals (e.g., mercury, chromium, lead, copper, zinc, arsenic), industrial solvents or surfactants (e.g., per- and polyfluoroalkyl substances (PFAS)), *Escherichia coli* bacteria, pharmaceuticals or personal care products, nutrients (e.g., nitrates and orthophosphates), and herbicides or pesticides.

2D-nanomaterial-based FET sensors are especially sensitive for detecting these various water contaminants with a low limit of detection (LOD) down to the $\times 10^{-9}$ M range as summarized in **Table 1**. Currently, the most commonly used 2D nanomaterials are graphene and its derivatives such as reduced graphene oxide (RGO), MoS_2 from the TMD family, and BP. These 2D nanomaterials act as the channel material for the sensing signal transduction, while specific probes are used for signal generation. Practically, various contaminants can be concurrently detected by a single channel material when conjugated with a specific probe for each individual contaminant. For example, graphene FET sensors have been demonstrated to detect heavy-metal ions,[65] bacteria,[66] and organic pollutants[67] in water. To detect mercury ions, the specific probes include DNA,[65b,68] organic molecules/compounds,[47a,65c,69] and proteins.[70] Selection of channel material and specific probes for targeted water pollutants are based on their sensing performance, cost, and stability. While the stability can be improved by protection of the sensor structure through passivation or packaging, the development of low-cost sensors that can measure water contaminants accurately in the field setting will represent a major development in water sensing.[7,71]

Technically, low-cost monitoring of water contaminants is promising when accompanied by scaled-up fabrication of FET/TFET sensor devices, but there are some hurdles regarding performance metrics that need to be overcome in real-world settings. The simultaneous detection of multiple types of contaminants with a high accuracy is the foremost performance metric that requires both classification of contaminant species and their quantification. Miniaturized FET/TFET sensor chips allow for their assembly in an array structure[80] integrated into a single substrate with multichannel data acquisition. Each sensor chip selectively detects one type of contaminant by conjugating the specific molecular probe. Continuous monitoring is another major challenge as the sensor array should be able to measure the real-time fluctuation of contaminant concentrations, which is dictated by the sensor recovery or regeneration capability (i.e., desorption of contaminants). One option to accelerate the recovery of FET/TFET sensors is to apply a repelling gate voltage[81] to weaken the electrostatic attraction between the probe and the analyte for fast desorption. In addition, biofilm formation on the sensor surface will degrade its performance and thus stability/lifetime as the microorganisms accumulate and prevent the contaminants from binding with probes. Interestingly, it has been shown that an electric field can inhibit the bacterial growth and thus can be used for treatment of bacterial biofilms,[82] suggesting that future FET/TFET sensors can potentially be protected against biofouling through an applied drain or gate electric field.

To rigorously test the graphene-based FET water sensing technology, a potential testbed of an intelligent, safe, and robust drinking-water system (Figure 4b) can be envisioned by coupling real-time sensors with smart filters, wireless communication, AI/ML, big data analytics, and geographic information systems. An intelligent drinking-water system could provide early warning to users when incidental water contamination elevates the water-contaminant concentration above the US Environmental Protection Agency (EPA) maximum contaminant level (MCL). If connected with real-time actuators, the system can automatically take measures to manage the situation and notify users who may be affected. As a result, smart drinking water systems could potentially ensure safety of public drinking water. Such a smart water system can also provide users with real-time water-quality information and allow water utilities to better monitor and control the water distribution system.

Another potential testbed for the graphene-based FET water sensor is the geospatial mapping of river-water quality with high spatio-temporal resolution, as demonstrated in a piloted project[83] that employs a commercial mobile sensing platform[84] equipped with GPS systems for geolocation, in which a variety of water parameters (e.g., pH, electrical conductivity, turbidity, temperature, concentrations of nitrate, dissolved oxygen, tryptophan, colored dissolved organic matter (CDOM), and chlorophyll) can be measured. These measurements are then converted into geospatial heatmaps (using geolocation) and displayed against a Google Maps rendition of the region. Geospatial imaging of water parameters offers unique abilities to pinpoint pollution sources and their impact on water

Table 1. Sensor structures and performances for detecting various water contaminants.

Water contaminant		Channel material	Specific probe	LOD	Ref.
Heavy-metal ions	Hg	Graphene	Au nanocluster	0.25×10^{-9} M	[65a]
			Aptamer	10×10^{-12} M	[65b]
			Ionophore	0.5×10^{-9} M	[65c]
		RGO	Thioglycolic acid	25×10^{-9} M	[47a]
			Polyfuran	10×10^{-12} M	[69a]
			Metallothionein type II protein	1×10^{-9} M	[70]
			N-[(1-pyrenyl-sulfonamido)-heptyl]-gluconamide	0.1×10^{-9} M	[69b]
			Single-stranded DNA	0.5×10^{-9} M	[68a]
			Nucleic acid	25×10^{-9} M	[68b]
		MoS_2	None	30×10^{-12} M	[41]
		BP	None	0.1×10^{-15} M	[40]
	Pb	Graphene	DNAzyme	0.02×10^{-9} M	[65d]
			G-rich DNA	0.8×10^{-9} M	[72]
		RGO	Reduced glutathione	10×10^{-9} M	[46]
		BP	Reduced glutathione	5×10^{-9} M	[73]
			Ionophore	4.8×10^{-9} M	[74]
			Cysteine	4.8×10^{-9} M	[75]
	As	Graphene	DNA	5×10^{-9} M	[65e]
		MoS_2	Ionophore	0.8×10^{-9} M	[76]
		BP	Dithiothreitol	1×10^{-9} M	[45]
	Cu	Graphene	Thiacalix[4]arene	1×10^{-6} M	[65f]
Nutrients	N	RGO	Benzyltriethylammonium chloride	18×10^{-9} M	[77]
	P	RGO	Ferritin	26×10^{-9} M	[78]
Bacteria	*E. coli*	Graphene	Anti-*E. coli* antibodies	10 cfu mL^{-1}	[66]
		RGO		10^3 cfu mL^{-1}	[79]
Pesticide	Chlorpyrifos	Graphene	Antichlorpyrifos antibodies	1.8×10^{-15} M	[67]

management.[2a] The sensors are regularly calibrated, and the measurements offer significant advantages over the conventional technique of point sampling, followed by laboratory measurements (typically followed in most of the world).

5. Conclusions and Future Outlook

2D nanomaterials are advantageous in FET/TFET sensor applications owing to their unique properties for superior sensing performance. Optimizing the sensing performance can be accomplished with a fundamental understanding of the semiconducting 2D nanomaterial channel for a given device structure. The rich selection of 2D nanomaterials offers a clear advantage for such optimization. Iterations between experiments and theoretical modelings such as density functional theory and statistical thermodynamics calculations have proven quite effective.[39] Computational AI/ML tools could enable high-throughput screening of existing 2D nanomaterials and the design of novel nanomaterials toward the best sensitivity. Once optimal 2D nanomaterials are predicted through computation, they can be synthesized and characterized to provide direct feedback for the material design phase to further improve sensing properties. Multiple technical hurdles also need to be overcome prior to large-scale deployment and commercialization of these sensors. Both fundamental research and translational research including scaled-up manufacturing are warranted. Fundamental research can advance our understanding of the sensing mechanism and process that enables the design and optimization of these sensors with desired performance, such as sensitivity, selectivity, and stability. Translation from a scientific concept to a commercial product poses further challenges for FET/TFET sensors in terms of device-to-device variation in large-scale fabrication, yield, and cost. Real-time water-quality monitoring represents a unique opportunity to demonstrate the power of the FET/TFET sensing platform and to illustrate the technology translation process by overcoming various technical challenges.

Political, economic, and social justice related challenges both plague and pose opportunities for water-quality sensors. Public drinking-water systems are highly regulated, and the regulations have been developed based upon balancing public health and economic burdens to monitor and treat water. While small drinking-water utilities have a disproportionate number of annual drinking-water violations in the USA,[85] pollutants such as arsenic may only need to be measured once every few years. The analytical methods for all drinking-water monitoring are highly controlled by federal-, state-, and even county-level authorities, and adoption of new analytical methods are rare, slow and represent a challenge for new technologies. In contrast, no regulations exist on the >40 million people in the USA who rely upon private wells for drinking water—except perhaps one required water-quality analysis at the time of home sales in some states. It is perhaps these unregulated applications at homes with private wells, schools, hospitals, and other locations where integration of sensor technology into POU devices that treat water at the tap may present the greatest opportunity for novel sensors. The POU market is >$20 billion per year and growing, and many companies seek to integrate networked sensors into treatment devices. Such a for-profit consumable device market provides a market where high-frequency testing is viewed beneficially. POU devices range in cost from a few hundred dollars to $1500, and there is some economical margin to integrate sensors. Sensors in POU devices must be durable and not require chemicals or frequent calibration.

The public has high concern about microbial and chemical agents in drinking water and is open to using new technologies that are validated by third parties, improve the quality of the water, and do not increase the cost of POU devices.[86] Whether in developed or developing countries,[87] there has been a rise in citizen science to fill occurrence gaps in water quality and provide rich openly-shared datasets.[88] Often spurred by pollution-related events (e.g., hydraulic fracturing), collecting and analyzing large numbers of samples can improve the public understanding of water-quality challenges.[87b] While colorimetric-based sensors or filter test strips are often used in these applications, the development and deployment of low cost and robust sensors could advance the capabilities of citizen science efforts to focus on microbial and chemical agents of greatest concern to the public. Many non-governmental organizations (NGOs) in the water, sanitation, and hygiene (WASH) sector that do utilize new technologies typically look toward three main criteria: 1) local capacity—does the technology fit the problem on a cultural and environmental scale and does the community have the ability to perform necessary maintenance,[89] 2) is there a legitimate proof of concept that demonstrates a working technology, and 3) is the technology sustainable (i.e., brings no unintended consequences). Care needs to be taken as a new technology is integrated into the mainstream public, as it has the potential to inadvertently alter the trust society has in political and regulatory structures. In addition, it can be difficult to draw direct connections between exposure to water-quality constituents and broader public health.[90] Therefore, public involvement in decision making related to the adoption of new technologies is paramount.[91]

Acknowledgements

The authors thank Dr. Supratik Guha of University of Chicago for offering insights into the river-water-quality monitoring testbed. J.H.C. and M.C.H. acknowledge the financial support from US National Science Foundation (NSF) Scalable Nanomanufacturing Program (NSF CMMI-1727846 and CMMI-2039268) and the NSF Future Manufacturing Program (NSF CMMI-2037026). P.W. acknowledges the financial support from the NSF Nanosystems Engineering Research Center on Nanotechnology-Enabled Water Treatment (EEC-1449500). This work was also supported by the Laboratory Directed Research and Development (LDRD) program from Argonne National Laboratory, provided by the Director, Office of Science, of the U.S. Department of Energy under Contract No. DE-AC02-06CH11357.

Conflict of Interest

J. H. Chen has a financial interest in NanoAffix Science LLC, which did not fund this work. All other authors declare no competing financial interests.

Keywords

2D nanomaterials, field-effect transistors, field testbed, real-time water sensors, technology translation

Received: September 2, 2021
Revised: October 1, 2021
Published online: December 18, 2021

[1] P. J. Vikesland, *Nat. Nanotechnol.* **2018**, *13*, 651.
[2] a) L. J. Klein, H. F. Hamann, N. Hinds, S. Guha, L. Sanchez, B. Sams, N. Dokoozlian, *IEEE Internet Things J.* **2018**, *5*, 4580; b) X. Zhang, A. Andreyev, C. Zumpf, M. C. Negri, S. Guha, M. Ghosh, in *2017 IEEE Conf. on Computer Communications Workshops (INFOCOM WKSHPS)*, IEEE, Piscataway, NJ, USA **2017**, pp. 78–84. https://doi.org/10.1109/INFCOMW.2017.8116356
[3] 2021 State of the Water Industry Report (American Water Works Association), https://www.awwa.org/Professional-Development/Utility-Managers/State-of-the-Water-Industry (accessed: October 2021).
[4] a) M. A. Edwards, A. Pruden, *Environ. Sci. Technol.* **2016**, *50*, 8935; b) K. J. Pieper, M. Tang, M. A. Edwards, *Environ. Sci. Technol.* **2017**, *51*, 2007; c) M. A. Edwards, A. Pruden, *Environ. Sci. Technol.* **2016**, *50*, 12057.
[5] M. Hanna-Attisha, J. LaChance, R. C. Sadler, A. C. Schnepp, *Am. J. Public Health* **2015**, *106*, 283.
[6] E. Olson, K. P. Fedinick, Natural Resources Defense Council Report: What's in Your Water? Flint and Beyond: Analysis of EPA Data Reveals Widespread Lead Crisis Potentially Affecting Millions of Americans, June 2016, https://www.nrdc.org/sites/default/files/whats-in-your-water-flint-beyond-report.pdf (accessed: October 2021).
[7] S. Mao, J. Chang, H. Pu, G. Lu, Q. He, H. Zhang, J. Chen, *Chem. Soc. Rev.* **2017**, *46*, 6872.
[8] U.S. Environmental Protection Agency, METHOD 6020B "Inductively Coupled Plasma—Mass Spectrometry", https://www.epa.gov/sites/default/files/2015-12/documents/6020b.pdf (accessed: October 2021)
[9] Palintest Water Analysis Technologies, SA1100 Scanning Analyzer, https://www.palintest.com/wp-content/uploads/2019/04/SA1100-Scanning-Analyzer.pdf (accessed: October 2021).
[10] Quasar Instruments, Andalyze AND1100 Fluorimeter, https://www.quasarinstruments.com/p-19165.aspx?searchEngineName=andalyze-and1100-fluorimeter-handheld-heavy-metal-water-tester (accessed: October 2021).

[11] a) A. H. Castro Neto, F. Guinea, N. M. R. Peres, K. S. Novoselov, A. K. Geim, *Rev. Mod. Phys.* **2009**, *81*, 109; b) K. S. Novoselov, A. K. Geim, S. V. Morozov, D. Jiang, Y. Zhang, S. V. Dubonos, I. V. Grigorieva, A. A. Firsov, *Science* **2004**, *306*, 666.
[12] a) S. Manzeli, D. Ovchinnikov, D. Pasquier, O. V. Yazyev, A. Kis, *Nat. Rev. Mater.* **2017**, *2*, 17033; b) B. Radisavljevic, A. Radenovic, J. Brivio, V. Giacometti, A. Kis, *Nat. Nanotechnol.* **2011**, *6*, 147; c) M. S. Fuhrer, J. Hone, *Nat. Nanotechnol.* **2013**, *8*, 146.
[13] a) L. Li, Y. Yu, G. J. Ye, Q. Ge, X. Ou, H. Wu, D. Feng, X. H. Chen, Y. Zhang, *Nat. Nanotechnol.* **2014**, *9*, 372; b) F. Xia, H. Wang, J. C. M. Hwang, A. H. C. Neto, L. Yang, *Nat. Rev. Phys.* **2019**, *1*, 306.
[14] G. Iannaccone, F. Bonaccorso, L. Colombo, G. Fiori, *Nat. Nanotechnol.* **2018**, *13*, 183.
[15] T. Liu, S. Liu, K.-H. Tu, H. Schmidt, L. Chu, D. Xiang, J. Martin, G. Eda, C. A. Ross, S. Garaj, *Nat. Nanotechnol.* **2019**, *14*, 223.
[16] a) Y. Cao, V. Fatemi, S. Fang, K. Watanabe, T. Taniguchi, E. Kaxiras, P. Jarillo-Herrero, *Nature* **2018**, *556*, 43; b) Y. Cao, V. Fatemi, A. Demir, S. Fang, S. L. Tomarken, J. Y. Luo, J. D. Sanchez-Yamagishi, K. Watanabe, T. Taniguchi, E. Kaxiras, R. C. Ashoori, P. Jarillo-Herrero, *Nature* **2018**, *556*, 80.
[17] H. Bergeron, D. Lebedev, M. C. Hersam, *Chem. Rev.* **2021**, *121*, 2713.
[18] M. E. Beck, M. C. Hersam, *ACS Nano* **2020**, *14*, 6498.
[19] a) D. Jena, *Proc. IEEE* **2013**, *101*, 1585; b) W. Cao, J. Jiang, J. Kang, D. Sarkar, W. Liu, K. Banerjee, in *2015 IEEE Int. Electron Devices Meeting (IEDM)*, IEEE, Piscataway, NJ, USA **2015**, pp. 12.3.1–12.3.4. https://doi.org/10.1109/IEDM.2015.7409682
[20] X. Xu, W. Yao, D. Xiao, T. F. Heinz, *Nat. Phys.* **2014**, *10*, 343.
[21] R. S. Muller, T. I. Kamins, M. Chan, *Device Electronics for Integrated Circuits*, John Wiley & Sons, New York **2003**.
[22] H. Sakaki, T. Noda, K. Hirakawa, M. Tanaka, T. Matsusue, *Appl. Phys. Lett.* **1987**, *51*, 1934.
[23] J. Kang, W. Cao, X. Xie, D. Sarkar, W. Liu, K. Banerjee, *Proc. SPIE* **2014**, *9083*, 908305.
[24] X. Cui, G.-H. Lee, Y. D. Kim, G. Arefe, P. Y. Huang, C.-H. Lee, D. A. Chenet, X. Zhang, L. Wang, F. Ye, F. Pizzocchero, B. S. Jessen, K. Watanabe, T. Taniguchi, D. A. Muller, T. Low, P. Kim, J. Hone, *Nat. Nanotechnol.* **2015**, *10*, 534.
[25] T. Roy, M. Tosun, X. Cao, H. Fang, D.-H. Lien, P. Zhao, Y.-Z. Chen, Y.-L. Chueh, J. Guo, A. Javey, *ACS Nano* **2015**, *9*, 2071.
[26] S. Agarwal, J. T. Teherani, J. L. Hoyt, D. A. Antoniadis, E. Yablonovitch, *IEEE Trans. Electron Devices* **2014**, *61*, 1599.
[27] G. H. Wannier, *Phys. Rev.* **1956**, *101*, 1835.
[28] a) F. Urbach, *Phys. Rev.* **1953**, *92*, 1324; b) W. Martienssen, *J. Phys. Chem. Solids* **1957**, *2*, 257; c) W. Martienssen, *J. Phys. Chem. Solids* **1959**, *8*, 294.
[29] a) S. M. Wasim, C. Rincón, G. Marín, P. Bocaranda, E. Hernández, I. Bonalde, E. Medina, *Phys. Rev. B* **2001**, *64*, 195101; b) Y. Pan, F. Inam, M. Zhang, D. A. Drabold, *Phys. Rev. Lett.* **2008**, 100, 206403; c) K. L. Chopra, S. K. Bahl, *Thin Solid Films* **1972**, *11*, 377.
[30] D. Jariwala, T. J. Marks, M. C. Hersam, *Nat. Mater.* **2017**, *16*, 170.
[31] S. Agarwal, E. Yablonovitch, *IEEE Trans. Electron Devices* **2014**, *61*, 1488.
[32] H. Zhang, W. Cao, J. Kang, K. Banerjee, in *2016 IEEE Int. Electron Devices Meeting (IEDM)*, IEEE, Piscataway, NJ, USA **2016**, https://doi.org/10.1109/IEDM.2016.7838512
[33] D. Sarkar, X. Xie, W. Liu, W. Cao, J. Kang, Y. Gong, S. Kraemer, P. M. Ajayan, K. Banerjee, *Nature* **2015**, *526*, 91.
[34] M. Li, D. Esseni, G. Snider, D. Jena, H. G. Xing, *J. Appl. Phys.* **2014**, *115*, 074508.
[35] E. Y. Sapan Agarwal, arXiv:1109.0096v3 **2014**.
[36] M. Chhowalla, D. Jena, H. Zhang, *Nat. Rev. Mater.* **2016**, *1*, 16052.
[37] a) M. A. Khayer, R. K. Lake, *IEEE Electron Device Lett.* **2009**, *30*, 1257; b) J. I. Pankove, *Phys. Rev.* **1965**, *140*, A2059 .
[38] D. Sarkar, K. Banerjee, *Appl. Phys. Lett.* **2012**, *100*, 143108.
[39] S. Cui, H. Pu, S. A. Wells, Z. Wen, S. Mao, J. Chang, M. C. Hersam, J. Chen, *Nat. Commun.* **2015**, *6*, 8632.
[40] J. Chang, H. Pu, S. A. Wells, K. Shi, X. Guo, G. Zhou, X. Sui, R. Ren, S. Mao, Y. Chen, M. C. Hersam, J. Chen, *Mol. Syst. Des. Eng.* **2019**, *4*, 491.
[41] S. Jiang, R. Cheng, R. Ng, Y. Huang, X. Duan, *Nano Res.* **2015**, *8*, 257.
[42] a) B. Zong, Q. Li, X. Chen, C. Liu, L. Li, J. Ruan, S. Mao, *ACS Appl. Mater. Interfaces* **2020**, *12*, 50610; b) F. Schedin, A. K. Geim, S. V. Morozov, E. W. Hill, P. Blake, M. I. Katsnelson, K. S. Novoselov, *Nat. Mater.* **2007**, *6*, 652.
[43] a) S. Cui, H. Pu, G. Lu, Z. Wen, E. C. Mattson, C. Hirschmugl, M. Gajdardziska-Josifovska, M. Weinert, J. Chen, *ACS Appl. Mater. Interfaces* **2012**, *4*, 4898; b) S. Cui, H. Pu, E. C. Mattson, G. Lu, S. Mao, M. Weinert, C. J. Hirschmugl, M. Gajdardziska-Josifovska, J. Chen, *Nanoscale* **2012**, *4*, 5887; c) S. Cui, Z. Wen, X. Huang, J. Chang, J. Chen, *Small* **2015**, *11*, 2305; d) S. Cui, Z. Wen, E. C. Mattson, S. Mao, J. Chang, M. Weinert, C. J. Hirschmugl, M. Gajdardziska-Josifovska, J. Chen, *J. Mater. Chem. A* **2013**, *1*, 4462; e) G. Lu, L. E. Ocola, J. Chen, *Adv. Mater.* **2009**, *21*, 2487.
[44] a) G. Zhou, J. Chang, H. Pu, K. Shi, S. Mao, X. Sui, R. Ren, S. Cui, J. Chen, *ACS Sens.* **2016**, *1*, 295; b) C.-W. Liu, C.-C. Huang, H.-T. Chang, *Anal. Chem.* **2009**, *81*, 2383; c) L. Shen, Z. Chen, Y. Li, S. He, S. Xie, X. Xu, Z. Liang, X. Meng, Q. Li, Z. Zhu, M. Li, X. C. Le, Y. Shao, *Anal. Chem.* **2008**, *80*, 6323.
[45] G. Zhou, H. Pu, J. Chang, X. Sui, S. Mao, J. Chen, *Sens. Actuators, B* **2018**, *257*, 214.
[46] G. Zhou, J. Chang, S. Cui, H. Pu, Z. Wen, J. Chen, *ACS Appl. Mater. Interfaces* **2014**, *6*, 19235.
[47] a) K. Chen, G. Lu, J. Chang, S. Mao, K. Yu, S. Cui, J. Chen, *Anal. Chem.* **2012**, *84*, 4057; b) S. Mao, G. Lu, K. Yu, Z. Bo, J. Chen, *Adv. Mater.* **2010**, *22*, 3521.
[48] a) E. Stern, R. Wagner, F. J. Sigworth, R. Breaker, T. M. Fahmy, M. A. Reed, *Nano Lett.* **2007**, *7*, 3405; b) N. Nakatsuka, K.-A. Yang, J. M. Abendroth, K. M. Cheung, X. Xu, H. Yang, C. Zhao, B. Zhu, Y. S. Rim, Y. Yang, P. S. Weiss, M. N. Stojanović, A. M. Andrews, *Science* **2018**, *362*, 319; c) M. Hinnemo, A. Makaraviciute, P. Ahlberg, J. Olsson, Z. Zhang, S. Zhang, Z. Zhang, *IEEE Sens. J.* **2018**, *18*, 6497; d) N. Gao, W. Zhou, X. Jiang, G. Hong, T.-M. Fu, C. M. Lieber, *Nano Lett.* **2015**, *15*, 2143.
[49] a) Y. Cui, Q. Wei, H. Park, C. M. Lieber, *Science* **2001**, *293*, 1289; b) J.-H. Ahn, S.-J. Choi, J.-W. Han, T. J. Park, S. Y. Lee, Y.-K. Choi, *Nano Lett.* **2010**, *10*, 2934; c) M. H. Jakob, B. Dong, S. Gutsch, C. Chatelle, A. Krishnaraja, W. Weber, M. Zacharias, *Nanotechnology* **2017**, *28*, 245503; d) J. Lee, J. Jang, B. Choi, J. Yoon, J.-Y. Kim, Y.-K. Choi, D. Myong Kim, D. Hwan Kim, S.-J. Choi, *Sci. Rep.* **2015**, *5*, 12286.
[50] K. Shoorideh, C. O. Chui, *Proc. Natl. Acad. Sci. USA* **2014**, *111*, 5111.
[51] a) J. Leem, M. C. Wang, P. Kang, S. Nam, *Nano Lett.* **2015**, *15*, 7684; b) M. T. Hwang, M. Heiranian, Y. Kim, S. You, J. Leem, A. Taqieddin, V. Faramarzi, Y. Jing, I. Park, A. M. van der Zande, S. Nam, N. R. Aluru, R. Bashir, *Nat. Commun.* **2020**, *11*, 1543.
[52] a) J. Kang, S. A. Wells, J. D. Wood, J.-H. Lee, X. Liu, C. R. Ryder, J. Zhu, J. R. Guest, C. A. Husko, M. C. Hersam, *Proc. Natl. Acad. Sci. USA* **2016**, *113*, 11688; b) X. Wang, P. Wu, *ACS Appl. Mater. Interfaces* **2018**, *10*, 2504; c) J. Kim, S. Kwon, D.-H. Cho, B. Kang, H. Kwon, Y. Kim, S. O. Park, G. Y. Jung, E. Shin, W.-G. Kim, H. Lee, G. H. Ryu, M. Choi, T. H. Kim, J. Oh, S. Park, S. K. Kwak, S. W. Yoon, D. Byun, Z. Lee, C. Lee, *Nat. Commun.* **2015**, *6*, 8294; d) Y. Yang, H. Hou, G. Zou, W. Shi, H. Shuai, J. Li, X. Ji, *Nanoscale* **2019**, *11*, 16; e) J. Ding, H. Zhao, Y. Zheng, Q. Wang, H. Chen, H. Dou, H. Yu, *Nanotechnology* **2018**, *29*, 095603; f) G. Hu, J. Kang, L. W. T. Ng, X. Zhu, R. C. T. Howe, C. G. Jones, M. C. Hersam, T. Hasan, *Chem. Soc. Rev.* **2018**, *47*, 3265.

[53] a) J. Kang, V. K. Sangwan, J. D. Wood, M. C. Hersam, *Acc. Chem. Res.* **2017**, *50*, 943; b) J. Zhu, M. C. Hersam, *Adv. Mater.* **2017**, *29*, 1603895.
[54] X. Sui, J. R. Downing, M. C. Hersam, J. Chen, *Mater. Today* **2021**, *48*, 135.
[55] J. Chang, G. Zhou, X. Gao, S. Mao, S. Cui, L. E. Ocola, C. Yuan, J. Chen, *Sens. Bio-Sens. Res.* **2015**, *5*, 97.
[56] G. C. Correa, B. Bao, N. C. Strandwitz, *ACS Appl. Mater. Interfaces* **2015**, *7*, 14816.
[57] Y.-G. Ha, K. Everaerts, M. C. Hersam, T. J. Marks, *Acc. Chem. Res.* **2014**, *47*, 1019.
[58] A. I. Abdulagatov, Y. Yan, J. R. Cooper, Y. Zhang, Z. M. Gibbs, A. S. Cavanagh, R. G. Yang, Y. C. Lee, S. M. George, *ACS Appl. Mater. Interfaces* **2011**, *3*, 4593.
[59] W. Li, O. Auciello, R. N. Premnath, B. Kabius, *Appl. Phys. Lett.* **2010**, *96*, 162907.
[60] Technology Readiness Assessment Guide, US Department of Energy, https://www.directives.doe.gov/directives-documents/400-series/0413.3-EGuide-04a/@@images/file (accessed: October 2021).
[61] U.S. National Science Foundation, https://www.nsf.gov/ (accessed: October 2021).
[62] J. Chen, S. Mao, G. Lu, *US 9676621*, **2017**.
[63] J. Namieśnik, A. Rabajczyk, *Chem. Speciation Bioavailability* **2010**, *22*, 1.
[64] a) Y. Xie, Y. Wang, V. Singhal, D. E. Giammar, *Environ. Sci. Technol.* **2010**, *44*, 1093; b) Y. Wang, J. Wu, Z. Wang, A. Terenyi, D. E. Giammar, *J. Colloid Interface Sci.* **2013**, *389*, 236.
[65] a) A. I. Ayesh, Z. Karam, F. Awwad, M. A. Meetani, *Sens. Actuators, B* **2015**, *221*, 201; b) J. H. An, S. J. Park, O. S. Kwon, J. Bae, J. Jang, *ACS Nano* **2013**, *7*, 10563; c) P. Li, B. Liu, D. Zhang, Y. Sun, J. Liu, *Appl. Phys. Lett.* **2016**, *109*, 153101; d) Y. Wen, F. Y. Li, X. Dong, J. Zhang, Q. Xiong, P. Chen, *Adv. Healthcare Mater.* **2013**, *2*, 271; e) Y. Wang, Y. Bi, R. Wang, L. Wang, H. Qu, L. Zheng, *J. Agric. Food Chem.* **2021**, *69*, 1398; f) Y. Takagiri, T. Ikuta, K. Maehashi, *ACS Omega* **2020**, *5*, 877.
[66] Y. Huang, X. Dong, Y. Liu, L.-J. Li, P. Chen, *J. Mater. Chem.* **2011**, *21*, 12358.
[67] S. Islam, S. Shukla, V. K. Bajpai, Y.-K. Han, Y. S. Huh, A. Ghosh, S. Gandhi, *Sci. Rep.* **2019**, *9*, 276.
[68] a) F. Tan, L. Cong, N. M. Saucedo, J. Gao, X. Li, A. Mulchandani, *J. Hazard. Mater.* **2016**, *320*, 226; b) E. Sharon, X. Liu, R. Freeman, O. Yehezkeli, I. Willner, *Electroanalysis* **2013**, *25*, 851.
[69] a) J. W. Park, S. J. Park, O. S. Kwon, C. Lee, J. Jang, *Analyst* **2014**, *139*, 3852; b) C. Yu, Y. Guo, H. Liu, N. Yan, Z. Xu, G. Yu, Y. Fang, Y. Liu, *Chem. Commun.* **2013**, *49*, 6492.
[70] H. G. Sudibya, Q. He, H. Zhang, P. Chen, *ACS Nano* **2011**, *5*, 1990.
[71] C. Liu, Z. Ye, X. Wei, S. Mao, *Electrochem. Sci. Adv.* **2021**, e2100137. https://doi.org/10.1002/elsa.202100137
[72] Y. Li, C. Wang, Y. Zhu, X. Zhou, Y. Xiang, M. He, S. Zeng, *Biosens. Bioelectron.* **2017**, *89*, 758.
[73] J. Chang, A. Maity, H. Pu, X. Sui, G. Zhou, R. Ren, G. Lu, J. Chen, *Nanotechnology* **2018**, *29*, 375501.
[74] P. Li, D. Zhang, J. Liu, H. Chang, Y. Sun, N. Yin, *ACS Appl. Mater. Interfaces* **2015**, *7*, 24396.
[75] A. Maity, X. Sui, H. Pu, K. J. Bottum, B. Jin, J. Chang, G. Zhou, G. Lu, J. Chen, *Nanoscale* **2020**, *12*, 1500.
[76] P. Li, D. Zhang, Y. Sun, H. Chang, J. Liu, N. Yin, *Appl. Phys. Lett.* **2016**, *109*, 063110.
[77] X. Chen, H. Pu, Z. Fu, X. Sui, J. Chang, J. Chen, S. Mao, *Environ. Sci.: Nano* **2018**, *5*, 1990.
[78] S. Mao, H. Pu, J. Chang, X. Sui, G. Zhou, R. Ren, Y. Chen, J. Chen, *Environ. Sci.: Nano* **2017**, *4*, 856.
[79] B. Thakur, G. Zhou, J. Chang, H. Pu, B. Jin, X. Sui, X. Yuan, C.-H. Yang, M. Magruder, J. Chen, *Biosens. Bioelectron.* **2018**, *110*, 16.
[80] a) I. Fakih, O. Durnan, F. Mahvash, I. Napal, A. Centeno, A. Zurutuza, V. Yargeau, T. Szkopek, *Nat. Commun.* **2020**, *11*, 3226; b) D.-I. Kim, T. Quang Trung, B.-U. Hwang, J.-S. Kim, S. Jeon, J. Bae, J.-J. Park, N.-E. Lee, *Sci. Rep.* **2015**, *5*, 12705.
[81] a) Q. Yue, Z. Shao, S. Chang, J. Li, *Nanoscale Res. Lett.* **2013**, *8*, 425; b) S.-H. Lee, J. S. Im, S. C. Kang, T.-S. Bae, S. J. In, E. Jeong, Y.-S. Lee, *Chem. Phys. Lett.* **2010**, *497*, 191.
[82] Y. W. Kim, S. Subramanian, K. Gerasopoulos, H. Ben-Yoav, H.-C. Wu, D. Quan, K. Carter, M. T. Meyer, W. E. Bentley, R. Ghodssi, *npj Biofilms Microbiomes* **2015**, *1*, 15016.
[83] P. Hirani, S. Balivada, R. Chauhan, G. Shaikh, L. Murthy, A. Balhara, R. C. Ponduru, H. Sharma, S. Chary, G. B. Subramanyam, S. Randhawa, T. Dutta, H. P. Gupta, A. Gupta, A. Haldar, A. Sarkar, I. Khan, S. Guha, in *2018 IEEE Sensors*, IEEE, Piscataway, NJ, USA **2018**, https://doi.org/10.1109/ICSENS.2018.8589560
[84] X. Zhang, A. Andreyev, C. Zumpf, M. C. Negri, S. Guha, M. Ghosh, in *2019 11th Int. Conf. on Communication Systems & Networks (COMSNETS)*, IEEE, Piscataway, NJ, USA **2019**, pp. 239–250. https://doi.org/10.1109/COMSNETS.2019.8711266
[85] M. Allaire, H. Wu, U. Lall, *Proc. Natl. Acad. Sci. USA* **2018**, *115*, 2078.
[86] J. Kidd, P. Westerhoff, A. D. Maynard, *NanoImpact* **2020**, *18*, 100220.
[87] a) P. Li, R. Tian, C. Xue, J. Wu, *Environ. Sci. Pollut. Res.* **2017**, *24*, 13224; b) A. Kinchy, S. Parks, K. Jalbert, *Environ. Plann. C: Gov. Policy* **2015**, *34*, 879; c) J. E. Givens, X. Huang, A. K. Jorgenson, *Sociol. Compass* **2019**, *13*, e12693.
[88] a) K. Jalbert, A. J. Kinchy, *J. Environ. Policy Plann.* **2016**, *18*, 379; b) C. Leeuwis, K. J. Cieslik, M. N. C. Aarts, A. R. P. J. Dewulf, F. Ludwig, S. E. Werners, P. C. Struik, *NJAS – Wageningen J. Life Sci.* **2018**, *86-87*, 146.
[89] a) V. Cornelissen,Project Manager – YEP Programmes, NGO Water Platform, TS Water & Maritiem. Netherlands Water Partnership., https://www.netherlandswaterpartnership.com/ (accessed: July 2021); b) B. Greiner, Global Programs Coordinator – Water for People, https://www.waterforpeople.org/ (accessed: July 2021).
[90] A. K. Jorgenson, *Int. Sociol.* **2009**, *24*, 115.
[91] K. Lyons, G. Scrinis, J. Whelan, in *Nanotechnology, Agriculture, and Food*, (Eds: D. Maclurcan, N. Radywyl), CRC Press, Boca Raton, FL, USA **2012**, Ch. 5.

Junhong Chen is currently a crown family professor of Molecular Engineering at Pritzker School of Molecular Engineering at the University of Chicago and lead water strategist at Argonne National Laboratory. Chen received his Ph.D. in mechanical engineering from the University of Minnesota in 2002. His research interest lies in molecular engineering of nanomaterials and nanodevices, particularly hybrid nanomaterials featuring rich interfaces and nanodevices for sustainable energy and environment. His approach is to combine multidisciplinary experiments with first-principles calculations to design and discover novel nanomaterials for engineering various sensing and energy devices with superior performance.

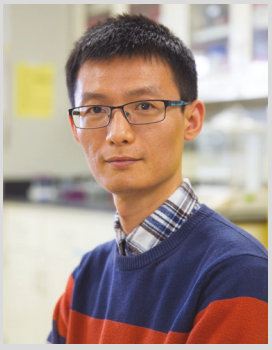

Haihui Pu received his Ph.D. from the University of Wisconsin-Milwaukee (UWM) in 2015. Before joining the University of Chicago as a Staff Scientist, he completed a Postdoctoral Appointment at UWM and worked as a Sensor Scientist for NanoAffix Science, LLC. Pu received his M.S. degree from Fudan University and his B.S. degree from Nanjing University of Science and Technology in China. His research focuses on the first-principles/molecular dynamics simulations and statistical thermodynamics modeling on novel 2D nanomaterials for environment and energy applications, which include field-effect transistor nanosensors for detecting various target analytes of interest and energy storage devices.

Mark C. Hersam is the Walter P. Murphy Professor of Materials Science and Engineering and Director of the Materials Research Center at Northwestern University. He also holds faculty appointments in the Departments of Chemistry, Applied Physics, Medicine, and Electrical Engineering. He earned a B.S. degree in Electrical Engineering from the University of Illinois at Urbana-Champaign (UIUC) in 1996, M.Phil. degree in Physics from the University of Cambridge (UK) in 1997, and a Ph.D. in Electrical Engineering from UIUC in 2000. His research interests include nanomaterials, nanomanufacturing, scanning probe microscopy, nanoelectronic devices, biosensors, and renewable energy.

Paul Westerhoff is a regents professor in the School of Sustainable Engineering and the Built Environment at Arizona State University and the fulton chair of Environmental Engineering. He joined ASU in 1995 and served as the Civil and Environmental Engineering Department Chair. He has over 320 journal publications and multiple patents on his research related to fate of nanomaterials in water, developing novel technologies for water and reuse treatment, and understanding reactions related to the fate of pollutants during treatment or in natural systems with a focus on oxo-anions, natural organic matter, and micropollutants.